EXECUTIVE SUMMARY

GSQC: Ground Segment Development for LEO to Ground Quantum Communication

(No.4000114938 /15/NL/RA/zk)

	Name/Title	Signature	Date
Prepared by	Thomas Scheidl IQOQI – Vienna		25.07.2018
Reviewed and approved by:	Rupert Ursin IQOQI Group Leader		25.07.2018
Technical management	Zoran Sodnik TEC-MME		26.7.18
IQOQI – Institute for Quantum Optics and Quantum Information Boltzmanngasse 3 1090 Vienna, Austria			

EUROPEAN SPACE AGENCY
CONTRACT REPORT

The work described in this report was done under ESA contract.
Responsibility for the contents resides in the author or
organisation that prepared it.

Page intentionally left blank

Table of Contents

Executive Summary

This executive summary document will summarize the highlights of the ESA-GSQC activity in which a ground segment for the reliable reception of (polarized) quantum optical signals from satellites has been developed. The goal was to develop a suitable versatile upgrade of the ESA-operated optical ground station (OGS) in Tenerife such that the optical link is dynamically adjusted and precisely maintained during a full satellite pass, thus facilitating future down links not only from quantum but also classical optical space terminals.

During the final measurements of the activity, the performance of the developed quantum ground receiver has been verified by means of downlink experiments from the Chinese Quantum Science Satellite “Micius” demonstrating the decoy-state quantum key distribution protocol using polarized weak laser pulses.

1. Description of the final satellite-ground experiment

The Chinese quantum science satellite will feature a single-photon source based on attenuated laser pulses at a pulse rate of 100 MHz and a wavelength of 850 nm. The quantum communication protocol for cryptographic key generation requires the intensity of the pulses to be chosen, such that on average approximately 0.5 photons per pulse will be sent towards the ground station. Additionally, the polarization state of every individual pulse will be randomly chosen between horizontal (H), vertical (V), diagonal (D) and anti-diagonal (A) polarization. At the receiving station, every incoming photon has to be randomly analyzed either in the H/V-basis or in the D/A-basis and the exact detection times have to be recorded with a temporal resolution better than 1 ns. For being able to match the transmitted and received photon pulses, the local time frames at the satellite and at the ground station have to be precisely synchronized. Therefore, a green beacon laser at 532 nm, 10 kHz pulse rate and 1 ns pulse width will be set in parallel to the quantum signal. Additionally, the beacon laser is supposed to be used as the reference beam for the tracking system on ground. Given the large divergence of the beacon laser to cover pointing inaccuracies of the satellite transmitter, the mean intensity of the beacon laser on ground is specified to be as low as 0.1 nW/m^2.

The Chinese satellite will generate a secure quantum key with different OGSs each at a time (e.g. the OGS in Tenerife and another OGS in China). Once this is achieved, the logical XOR combination of the two individual keys can be used to device, in an absolutely secure way, a common key between the two ground stations. This is called “Quantum key relay protocol”.

2. Requirements for the quantum receiver and tracking system

The following list summarized the relevant characteristics of the Chinese satellite, imposing certain requirements on the quantum ground receiver, which are subsequently summarized in Table 1.

1. Orbit:
    - sun-synchroneous:
      570 km height, 97.79° inclination, local time at decending node is 00:00h
    - 500 m prediction accuracy

2. Tracking beacon downlink:
    - 532 nm, 10 kHz pulse rate, 1 ns pulse width
    - 0.1 nW/m^2 minimal average intensity on ground (specified by Chinese partners)

3. Tracking beacon uplink:
    - 671 nm CW Laser
    - Output power: 3 W
    - 3 mrad divergence

4. Quantum signal:
    - 850 nm, 100 MHz pulse rate, 100 ps pulse width
    - Diffraction limited divergence

5. OGS:
    - Aperture diameter d_{OGS}=1016 mm
    - Diameter of central obscuration d_{obs}=330 mm
    - Focal length $f_{Cassegrain}$=13300 mm
    - Dynamic pointing error approx. 0.3 mrad

6. Protocol:
    - Polarization measurement randomly in H/V or D/A basis
    - Polarization contrast better than 1:200
    - Timing resolution for quantum signal detectors better than 1 ns
    - Dark count of quantum signal detectors smaller than 200 cps

Requirements Matrix		
Tracking system	Wavelength	532 nm
	$FOV_{tracking}$	> 3 mrad
	Angular resolution	< 10 µrad
	Optical sensitivity of camera	< 33 pW @ 532 nm
	Closed-loop bandwidth	> 100 Hz
Uplink	Wavelength	671 nm
	Divergence	3 mrad divergence
	Output power	3W
Quantum detection	$FOV_{quantum}$	50-100 µrad
	Polarization contrast	> 1:200
	Random basis choice	H/V and D/A
	Timing resolution	< 1 ns
	Dark counts	< 200 cps

Table 1 – Requirement Matrix

3. Design of the quantum communication receiver package

The final design of the quantum communication receiver package is shown in Figure 1. Since we aimed at a most compact setup, which is compliant with the mounting attachments at the Cassegrain focus of the OGS telescope, we chose to implement the optical path mainly with 1” optical elements. When using 1” optical elements it is immediately clear that an unvignetted $FOV_{tracking}$ of > 3 mrad cannot be guaranteed. As a solution, the wide-field telescope (WFT) and camera (WFC), attached

directly to the tube of the OGS telescope and aligned to its optical axis, will be utilized as a coarse pointing system (CPS). The WFT has a diameter of d_{WFT}=180 mm and a focal length of f_{WFT}=1800 mm. The WFC in the focal plane of the WFT covers a FOV of approximately 3.7 mrad and hence is compliant with the $FOV_{tracking}$ requirement for the tracking system as given in Table 1. The pixel size of the WFC is 23x23µm^2 corresponding to an angular resolution of roughly 10 µrad. In the first step of the tracking loop, the CPS will adjust the OGS telescope pointing, such that the satellite becomes visible within the FOV of an additional fine-pointing system (FPS). Furthermore, the intensity of the tracking beacon from the satellite is comparable to a star with magnitude 4 and hence should be bright enough to be reliable captured be the WFC.

The FPS and the quantum communication receiver package will be installed in the Cassegrain focus of the OGS telescope. A folding mirror directs the incoming beam into the plane of our setup. A collimation lens (f_{col}=125 mm) in combination with the focal length of the OGS telescope (f_{tel}=13300 mm) results in a collimated beam with a diameter of d_{col}=9.55 mm, corresponding to a magnification of roughly 100. The tip/tilt mirror of the FPS is placed in the pupil plane, 125 mm after the collimation lens and reflects the incoming light by 90 deg towards a dichroic mirror. The dichroic mirror reflects the quantum signal at 850nm towards the quantum “Detection” sub-system and transmits the beacon laser at 532 nm towards the “Timing+Tracking” sub-system.

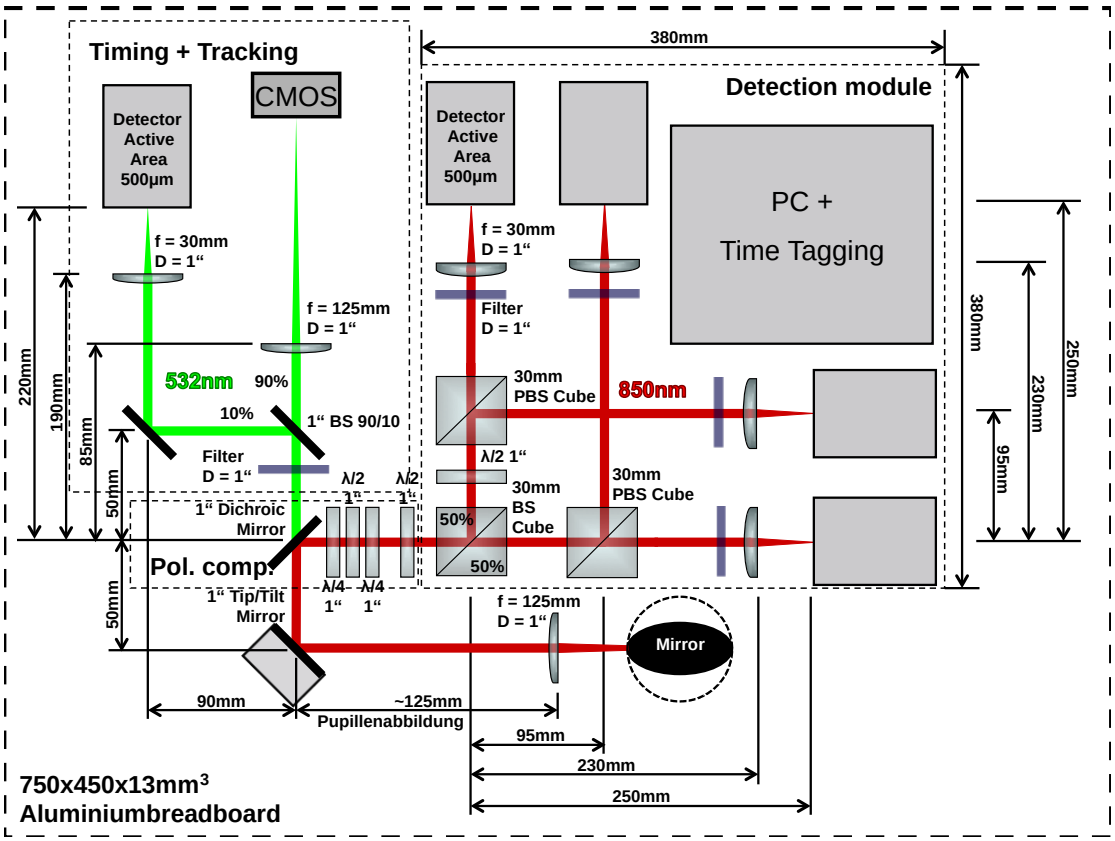

Figure 1 – Design of the quantum communication receiver package for the OGS telescope in Tenerife.

4. “As-built” documentation and performance verification

After the successful completion of the design phase, the quantum ground receiver was built and setup in the laboratory for initial tests. In a next step (as summarized in this Chapter), the desired performance was verified utilizing a static horizontal free-space link between La Palma and Tenerife. Furthermore, a step-by-step optical alignment manual as well as a user manual for the image-stabilization software have been developed (see TN2).

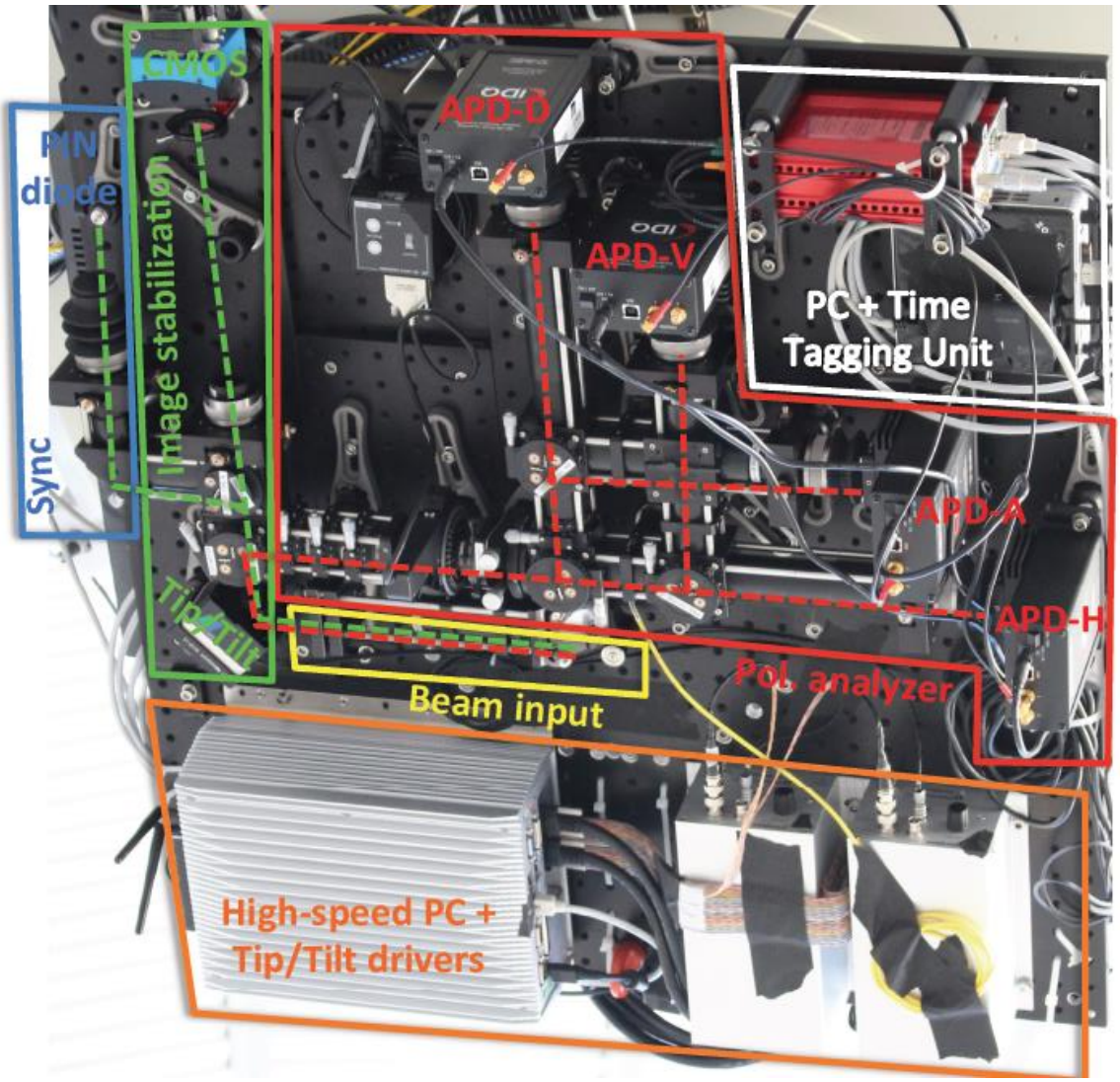

Figure 2 – The picture shows the "as-built" after the completion of the beam path alignment. The yellow box indicates the location of the beam input to the quantum receiver module. The green and red dashed lines indicate the beam path of the 532nm pulsed beacon laser and the 850nm quantum signal, respectively. Both beams hit the tip/tilt mirror in the pupil plane of the collimation lens (placed inside the yellow beam input box). The beacon laser beam is split at a 90/10 beam splitter, such that 10% of the signal is guided to a PIN diode (blue box) for timing synchronization purpose, whereas 90% of the signal is focused onto the CMOS camera. The images of the CMOS camera are processed by the high-speed PC (orange box), which adjusts the tip/tilt mirror (green box) via the tip/tilt voltage drivers (orange box) accordingly. The red box shows the quantum polarization analyzing sub-system with the four single photon detectors (APDs) for detecting H, V, D and A polarized photons, respectively. The white box shows the PC and time tagging unit needed for storing the detection events during the execution of the quantum communication protocol.

4.1. Performance verification – Image-stabilization subsystem

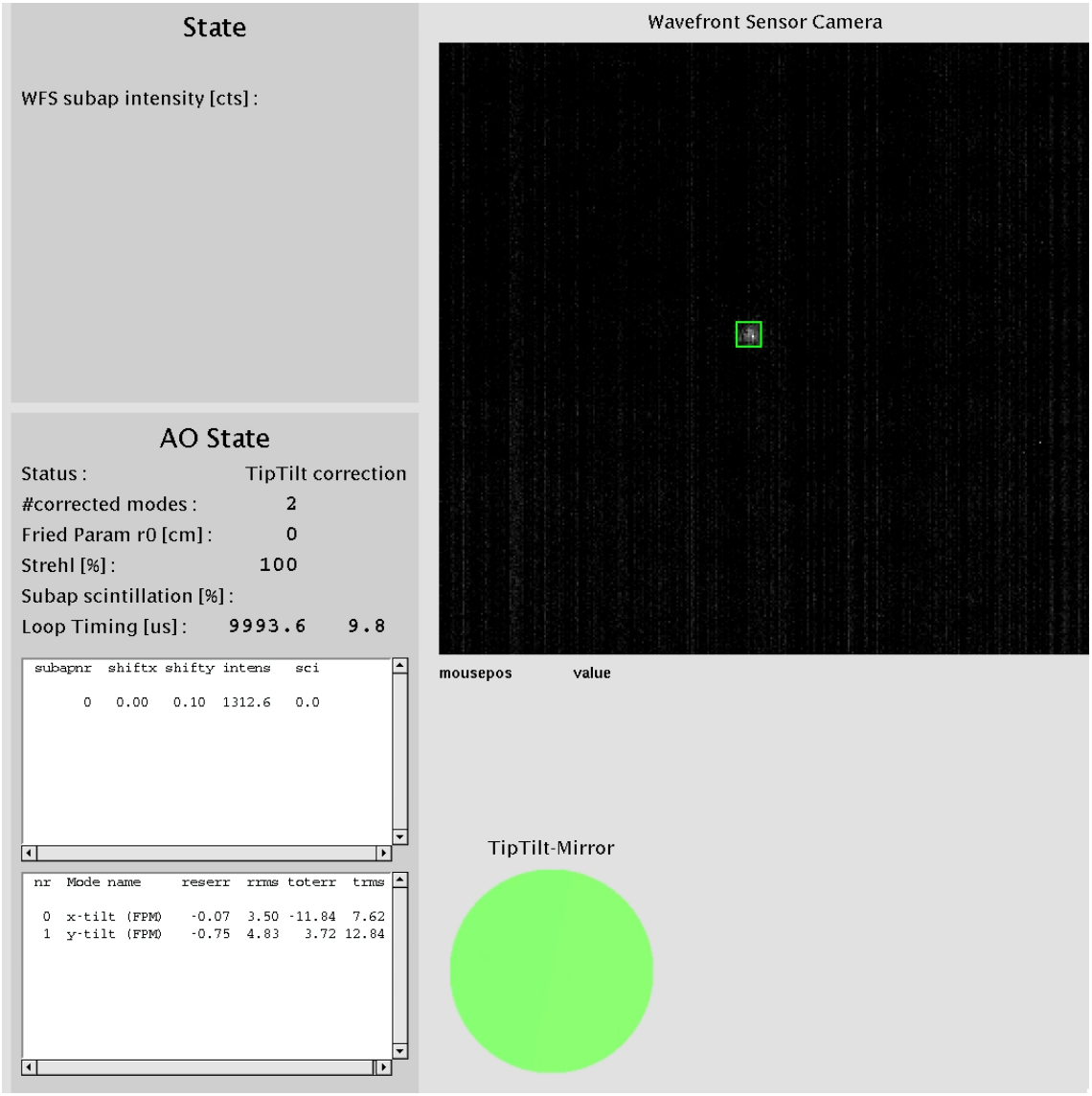

Figure 3 – This picture shows a screen-shot of the tip/tilt software during operation at a beacon intensity level of ***20 pw/m2****. The red ellipse indicates the closed-loop timing, which was 10000µs, corresponding to* ***100Hz closed-loop bandwidth****.*

4.2. Performance verification – Polarization analysis subsystem

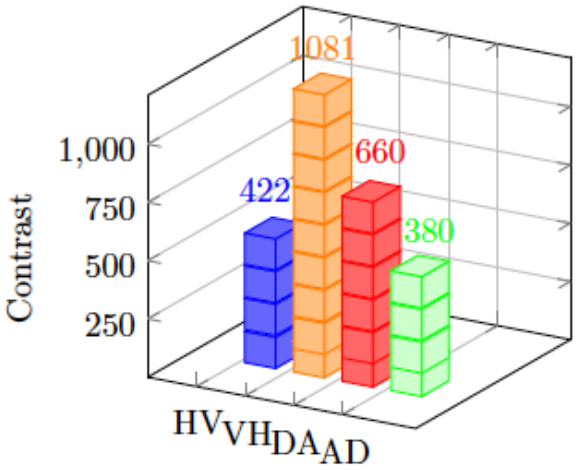

	Contrast
HV	422 ± 47
VH	$1{,}081 \pm 297$
DA	660 ± 45
AD	380 ± 114

Figure 4 – Measured polarization contrasts of our quantum communication receiver module. The results clearly show that the ***requirement of C>1:200 could easily be fulfilled****.*

5. Stellar tracking and dynamical satellite tracking tests

In a next measurement campaign, we investigated the performance of our setup by using bright stars as well as sun-illuminated LEO satellites. During these measurements the main focus was on the tracking performance and on software-compatibility checks between the image-stabilization and the OGS-GUI computer.

5.1. Performance verification – Stellar tracking and FSM desaturation

For investigating the performance of the desaturation algorithm we tracked stars using the OGS-GUI computer and applied arbitrary telescope offsets (see Figure 5-7).

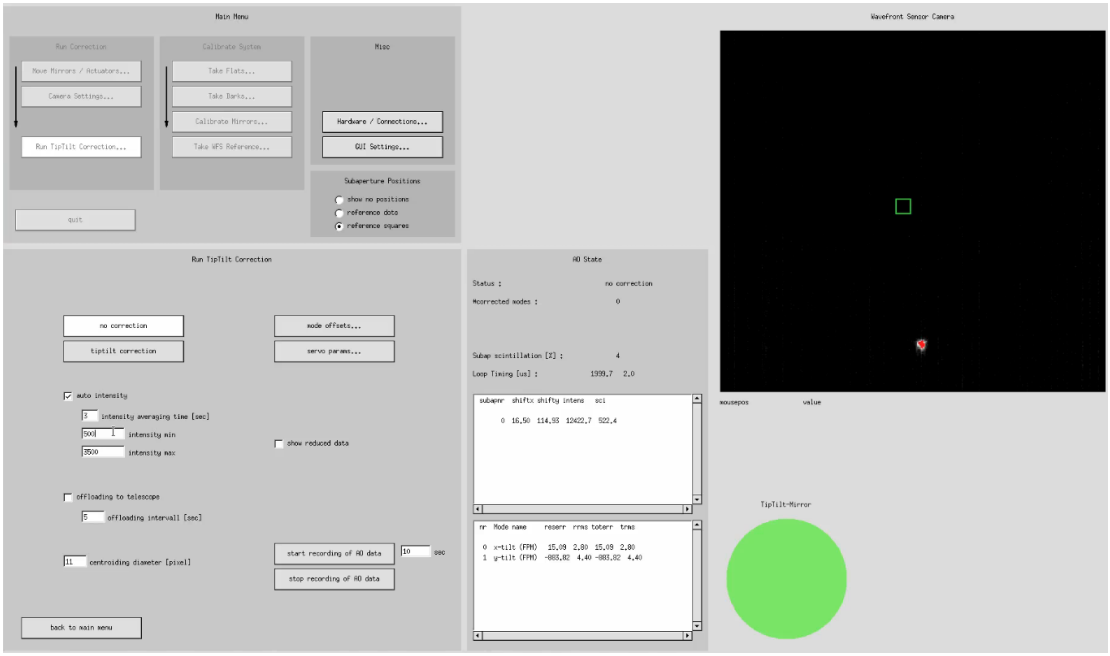

Figure 5 – The reference position is indicated by the green square in the center of the CMOS image. After applying an offset to the telescope of 250µrad at the RA axis and 40µrad at the DEC axis, the spot deviated from the reference position at the CMOS chip roughly 114 pixel along the Y-axis and 18 pixel along the X-axis.

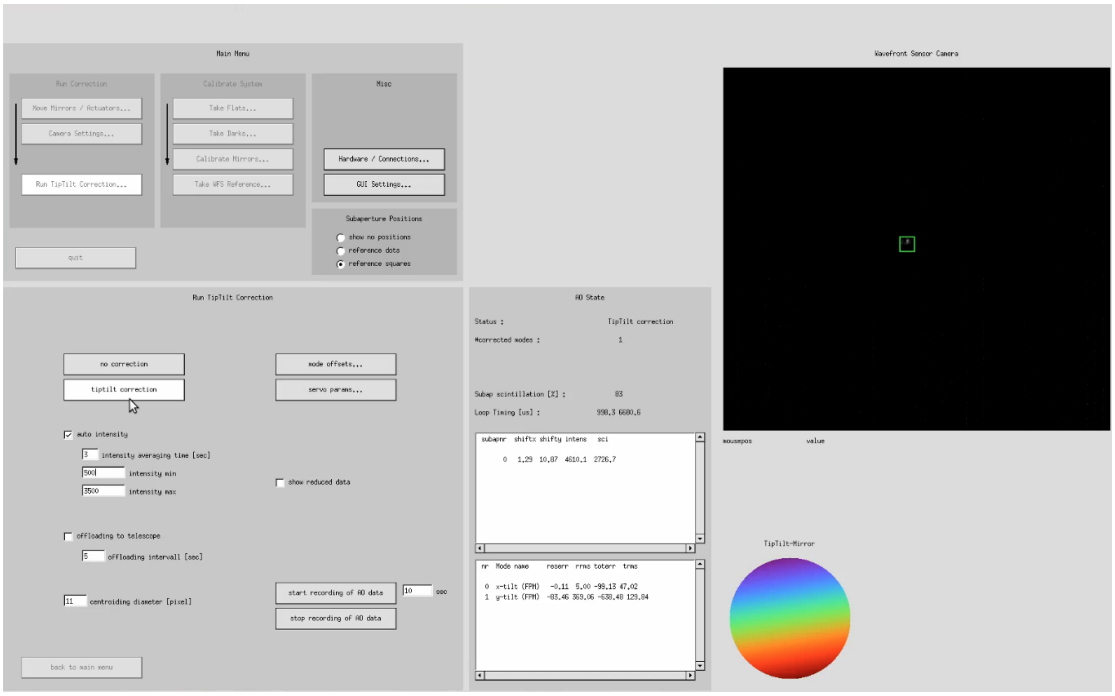

Figure 6 – When switching on the tip/tilt correction only, the spot is moved back to the reference position. The FSM stroke, however, nearly reaches its maximum, as indicated by the color-coded graduator for the FSM stroke.

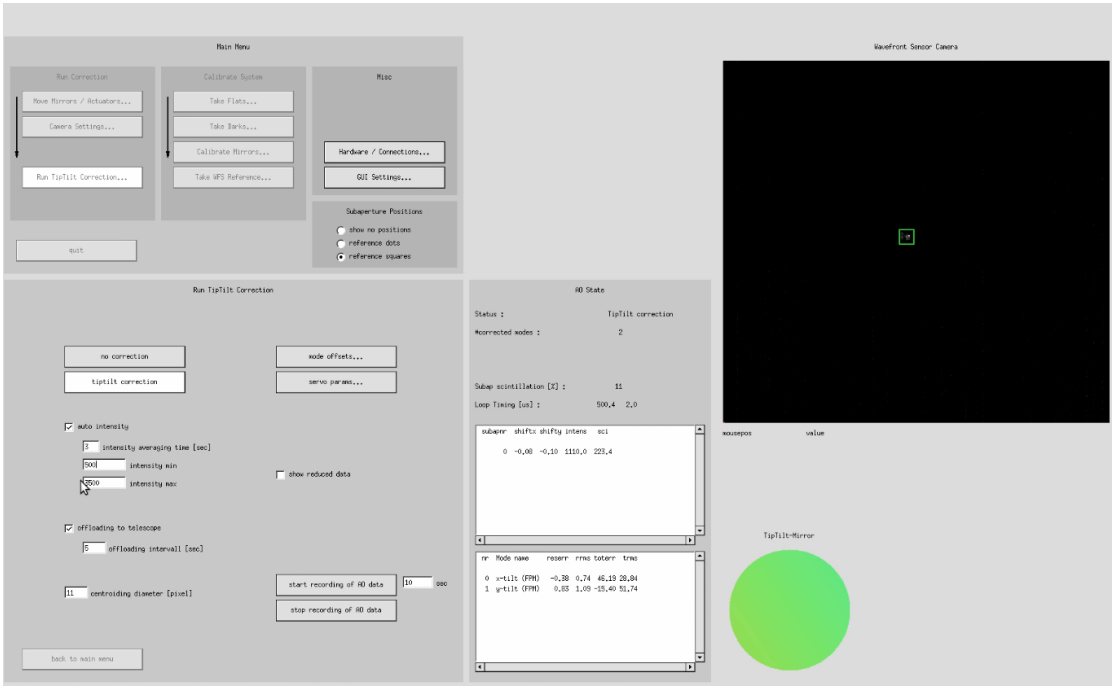

Figure 7 – When activating the desaturation mechanism, our image stabilization software is sending the corresponding offset commands to the OGS-GUI computer, which applies the offset to the telescope accordingly. The FSM stroke gets desaturated, as can be seen by the uniformly colored graduator for the FSM stroke.

5.2. Performance verification – Satellite tracking tests

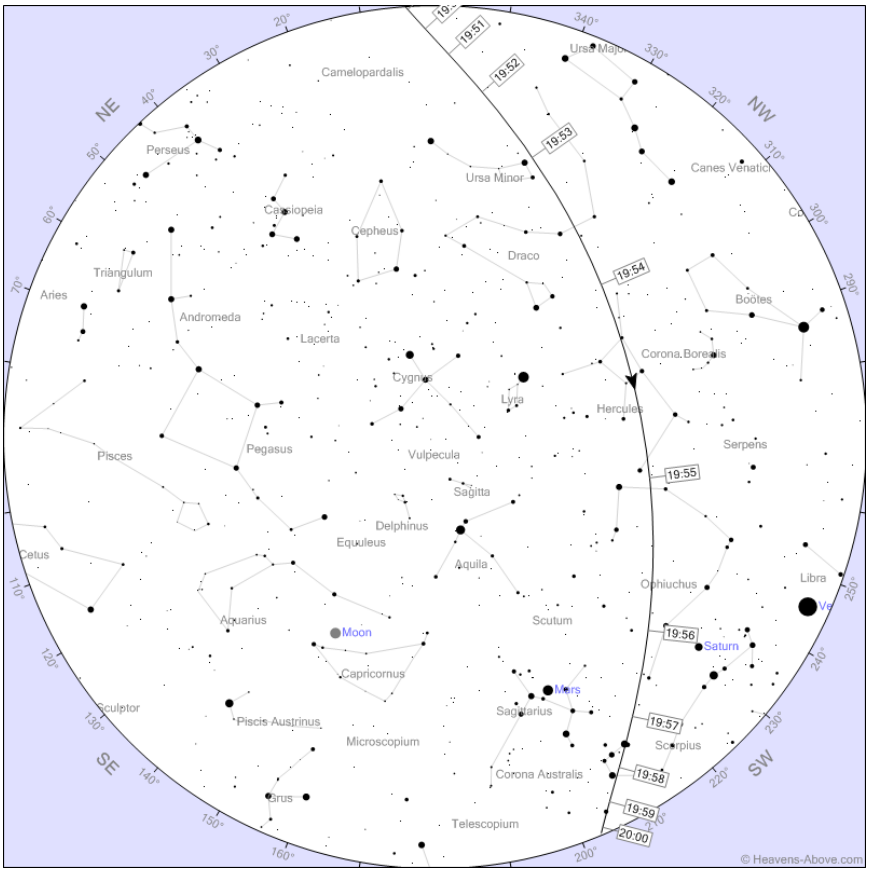

Figure 8 – Pass details of the Meteor 1-28 rocket satellite.

Having demonstrated the desired functionality of the FSM desaturation mechanism, we tested our system via dynamical tracking LEO satellites (e.g. Meteor 1-28 Rocket satellite, see Figure 8). We captured the spot of the satellite on the coarse pointing camera (wide-field-camera of the OGS telescope) and moved it into the fine-pointing field-of-view. We then activated the image stabilization software and observed the count-rate of the sun-illuminated satellite at our 4 single-photon detectors in the polarization analyser subsystem (see Figure 9).

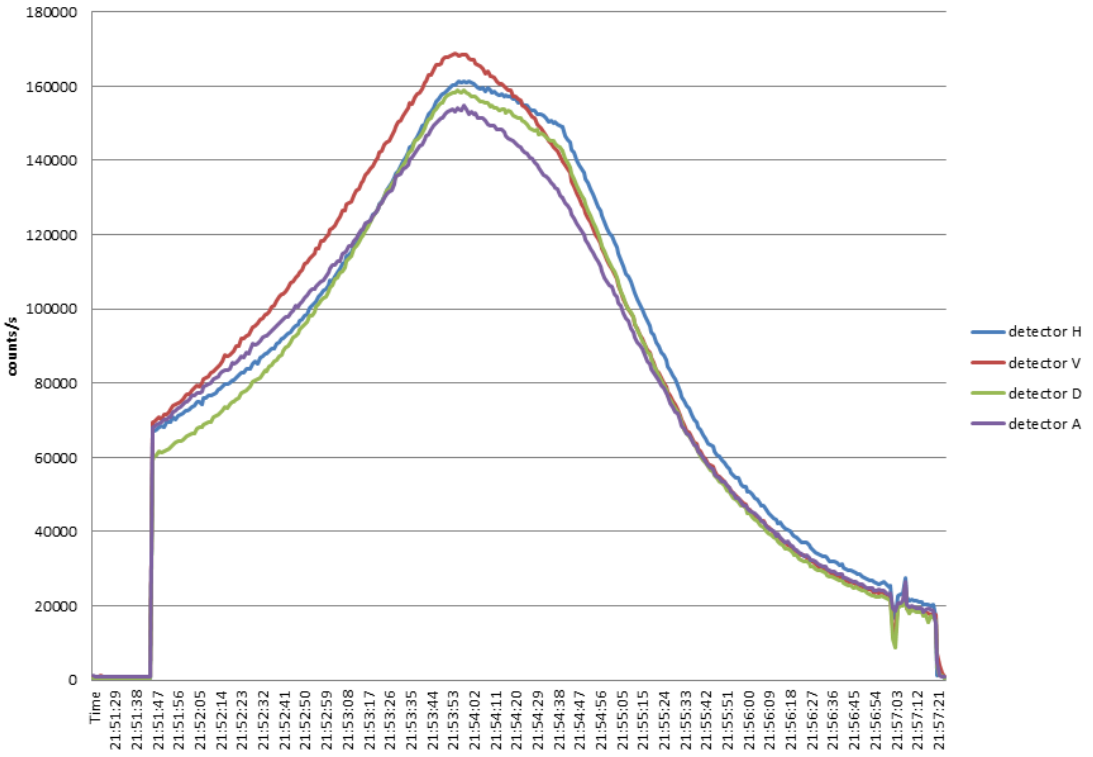

Figure 9 – Counts per second at the 4 single photon detectors in the polarization analyzer sub-system while tracking the Meteor 1-28 Rocket satellite.

6. Final measurements – Downlinks from "Micius"

The final measurements can be divided into four phases: i) satellite tracking tests using the green beacon laser sent from the Chinese satellite, ii) verification of the polarization compensation performance based on a strong optical signal sent from the satellite, iii) execution of the decoy-state QKD protocol based on a pre-programmed random sequence at the satellite for modulating the polarization and intensity of the quantum signal (offline QKD) and iv) execution of the final decoy-state QKD protocol based on a random sequence, which was generated in real-time during the satellite pass (online QKD). The results presented in this document have been obtained during a measurement campaign executed in the period between the 3rd and 19th of April 2018.

6.1. Tracking Tests

Figure 10 shows the actual tracking performance of the first satellite pass. The orange and blue lines correspond to the offset of the spot's center of mass from the reference position at the fine-pointing camera along the x- and y-axis, respectively. As explained above, in the first half of the pass we realized that there must be an error with the signs for the offset commands the OGS-GUI computer was sending to the TTC. As a consequence, we struggled a lot with the AVAS software to move the spot into the fine-pointing FOV despite the sign errors. During our attempts, the spot sometimes crossed the fine-pointing FOV. However, these FOV crossings, indicated by the spikes in the graph, happened to quickly for the tip/tilt system to capture the spot. However, finally (around second 260) we managed to capture the spot in the fine-pointing FOV and close the tip/tilt loop. For the rest of the pass the satellite could nicely be tracked with a resolution of better than 2 pixel on the fine-pointing camera, corresponding to a resolution of better than 4.4µrad.

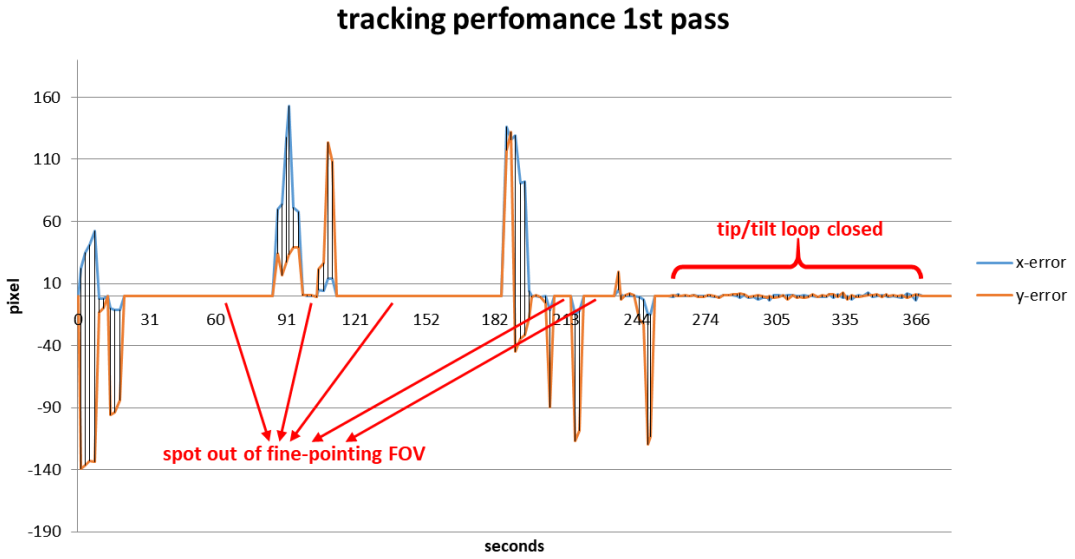

Figure 10 – Tracking performance of the first satellite pass. The plot shows the difference of the spot's centre of mass from the reference position at the fine pointing camera along the x- and y- axis, respectively.

For comparison, Figure 11 shows the tracking performance for a typical satellite pass, after the problems with the sign-errors for the offset commands have been resolved. At the beginning of the pass, the spot was moved into the fine-pointing FOV with the help of the AVAS software and the tip/tilt loop was closed immediately. Since also the offloading worked properly, the satellite was automatically tracked for the rest of the satellite pass without any further manual interaction.

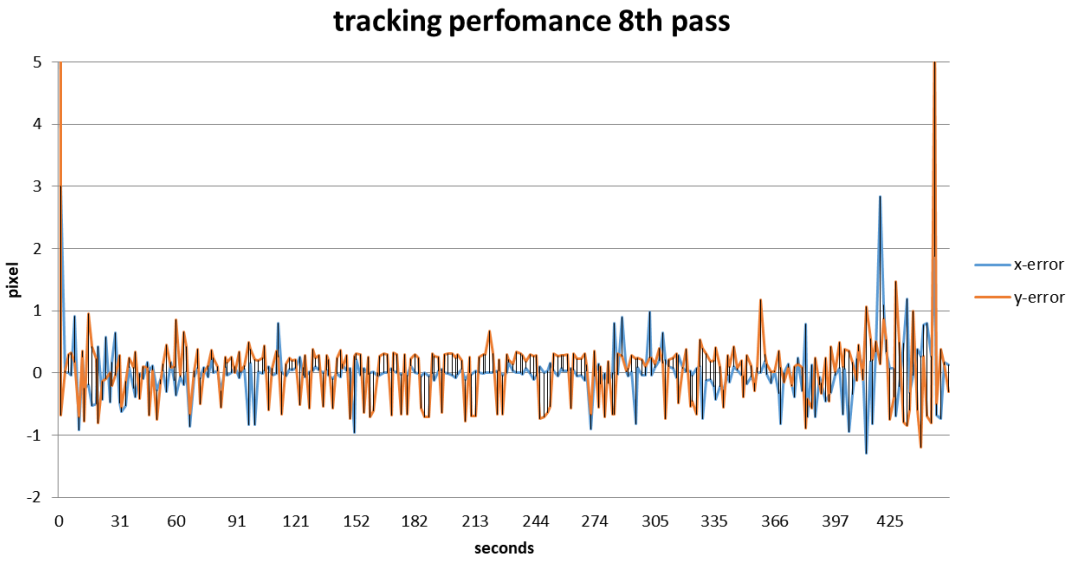

Figure 11 – Tracking performance for a typical satellite pass, after the sign-errors have been corrected and the offset commands have been correctly applied.

6.2. Polarization Tests

The polarization test was performed during the satellite pass starting on April 11th at 0:43 UTC. The Chinese satellite was sending a “strong” H polarized quantum signal in parallel to the beacon laser. The average number of photons arriving on ground was approximately 6.5x10^{8}, such that we introduced and 30dB neutral density filter into our receiving setup in order to not saturate our detectors.

If everything worked correctly, there should have been a high contrast between the counts at the “H” and “V” detectors. However, as can be seen in Figure 12, we found a high contrast between the “D” and “A” detectors, indicating a problem with the polarization compensation subsystem. Nevertheless, the contrast between the “D” and “A” detectors stayed quite constant over time, indicating that the polarization compensation scheme seems to work properly in general and only the initial rotation angle position of the HWP was only calibrated wrongly. During the course of the pass (roughly between second 340 and 440, see Figure 12) we manually added offsets to the HWP rotation angle in order to restore a good contrast between the “H” and “V” detector and noted the offset. The next day, we investigated the issue and found a problem with the motorized HWP rotation stage. It turned out that due to incorrectly set parameters for rotation velocity and acceleration of the motorized stage, the actual HWP angle did not match the values shown in the software.

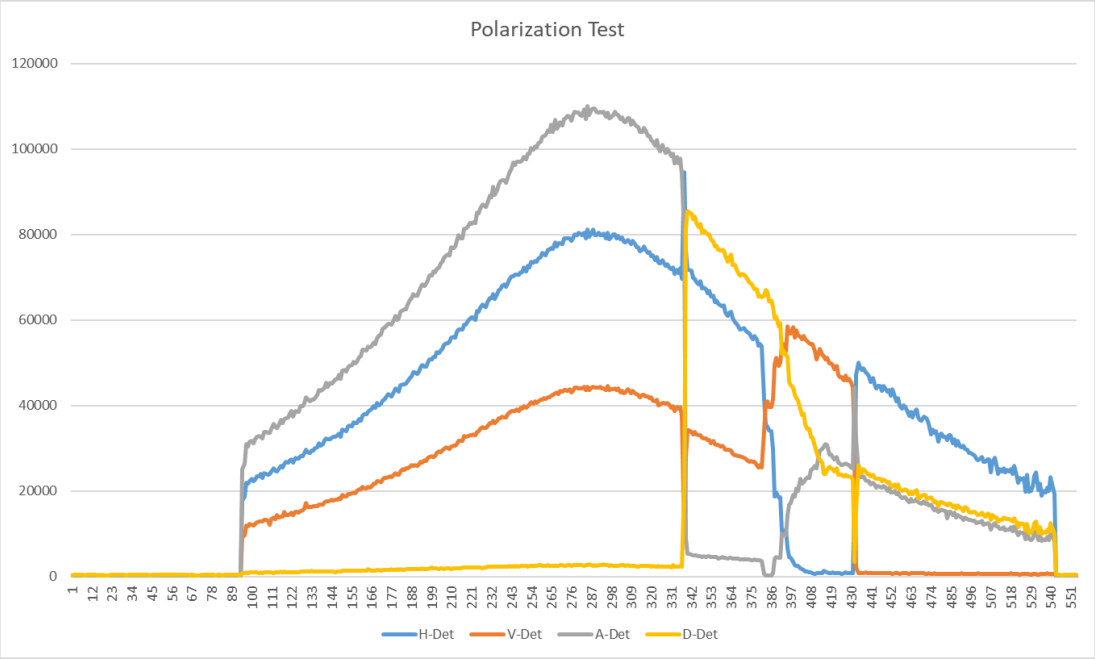

Figure 12 – Counts per second at the 4 single photon detectors (H, V, A, D) in the polarization analyser subsystem during the satellite pass.

We could easily fix this problem during day and repeated the polarization test during the pass starting on April 13th at 01:33 UTC. The results are shown in Figure 13. This time there was good contrast between the counts at the “H” and “V” detector from the beginning and could be maintained throughout the satellite pass. The contrast values (without subtracting background counts) are also shown in Figure 13. Since the detectors start saturating at around 100kHz count rate and taking into account that background counts are not subtracted, the obtained contrast-values between 50 and 100 could be considered sufficient and the polarization tests completed successfully.

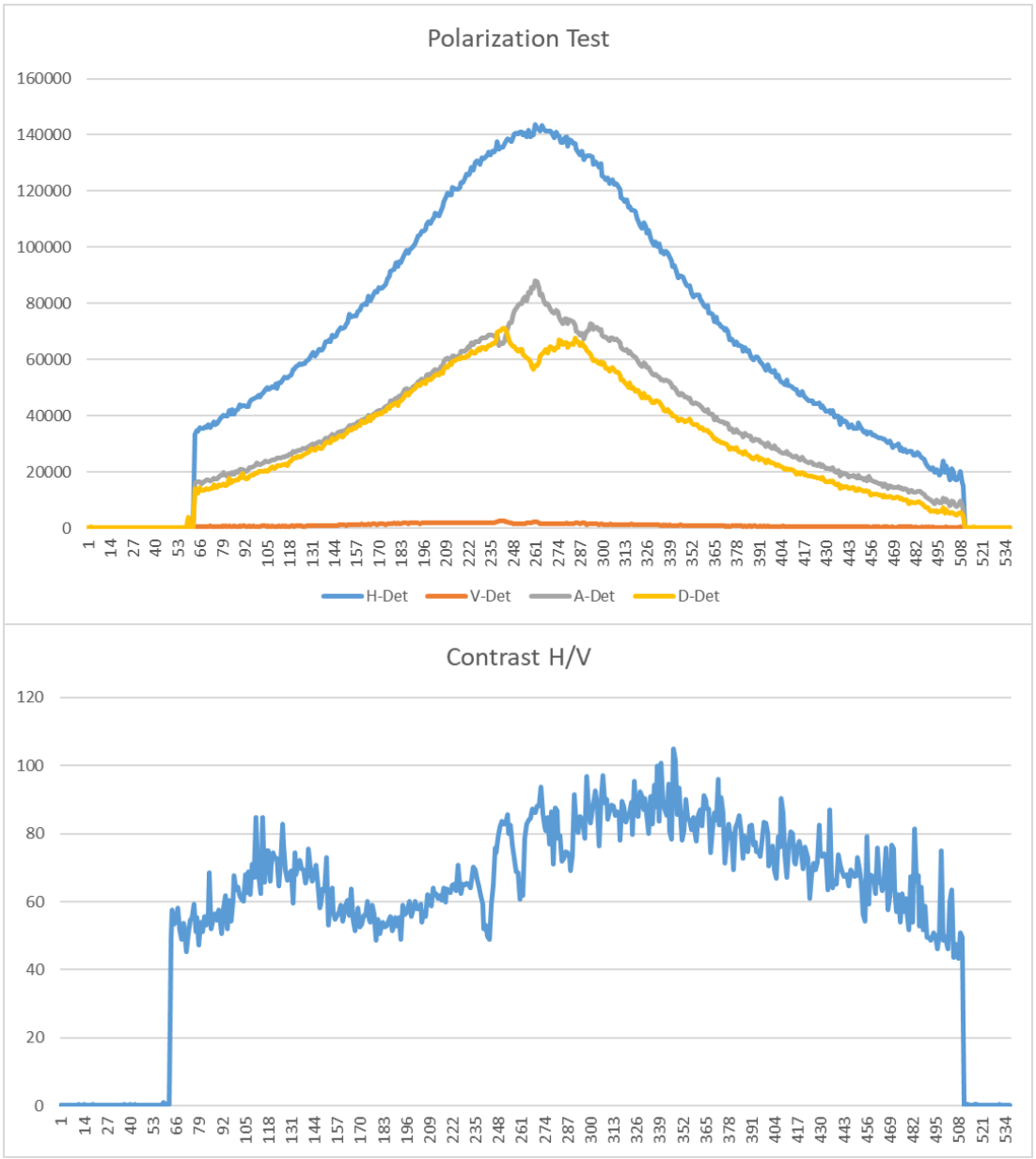

Figure 13 – Up: Counts per second at the 4 single photon detectors (H, V, A, D) in the polarization analyser subsystem. Down: Contrast in the H/V polarization basis (i.e. counts at the H detector divided by counts at the V detector) without background subtracted.

6.3. Offline QKD

After the successful tracking and polarization tests we proceeded with the first offline QKD downlinks. Offline QKD means, that the decoy-state QKD transmitter at the satellite modulates the intensity and the polarization of the quantum signal based on a preprogrammed and known random sequence, which allows performing key sifting and analyzing the quantum bit error rate (QBER) without the need to

communicate classically with the satellite for exchanging information about the polarization measurement bases and the intensity level (signal or decoy intensity level) of the generated quantum states. The first offline QKD measurements have been performed at the satellite pass starting on April 14th at 01:10h UTC.

Figure 14 shows the measured photon rate at the 4 single photon detectors after the sifting process, i.e. only signal-state photons that were measured in the same polarization basis as they have been generated at the satellite are taken into account. Consequently, the sum of the counts at the four detectors corresponds to the actual sifted key rate and amounts to approximately 160kbit/s at highest elevation of 89°. Taking into account the pulse rate of the decoy-state source at the satellite of 100MHz, the fraction of signal pulses of 0.5, the mean photon number of signal states of 0.8 and the basis reconciliation factor of 0.5 the total attenuation of the quantum channel (including losses in the receiving module and detector efficiencies) is approximately 21dB.

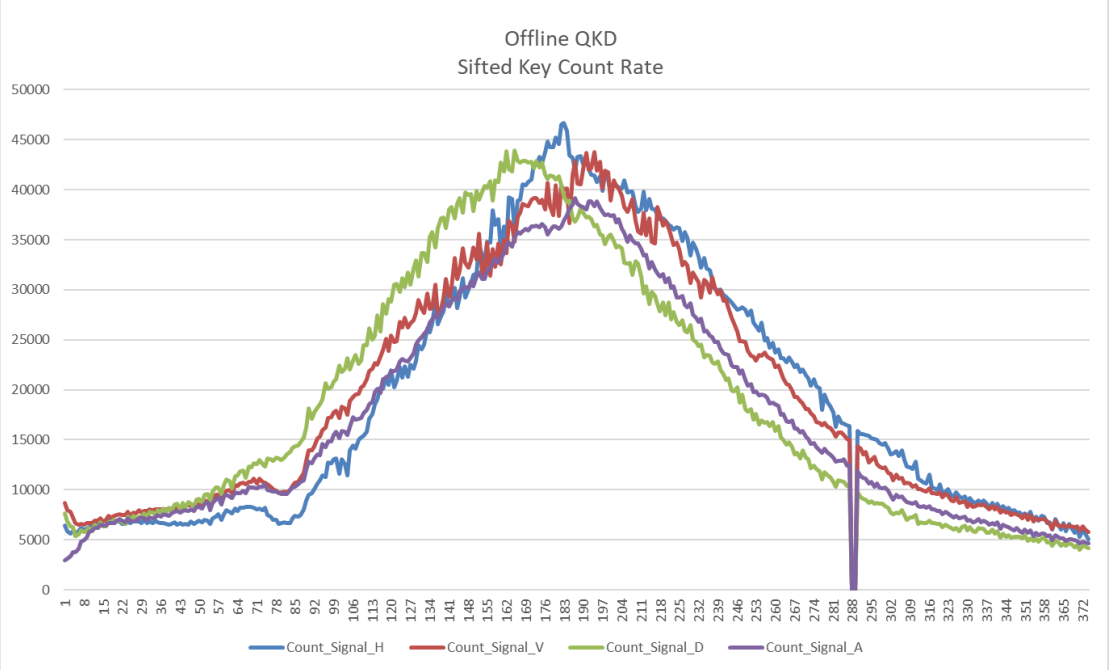

Figure 14 – Sifted key counts at the four single photon detectors in the quantum receiving module during the satellite pass for the first offline QKD test.

The average QBER was 0.7%, the average sifted key rate was 90kbit/s and the total sifted key lengths amounts to 25Mbit. Based on this values, a secure key can be generated at an average rate of approximately 30kbit/s and the total amount of the secure key of the whole satellite pass amounts to roughly 8Mbit. We have obtained similar results with the offline QKD test executed during the satellite pass starting on April 15th at 00:49h UTC. This pass had a maximum elevation of 40° and thus, the average rates and total lengths of sifted and secret key are of course less compared to

the previous close-to-zenith pass. We obtained again an average QBER of 0.7%, an average sifted key rate of 54kbit/s and a total of 15Mbits of sifted key. This results in a secret key at an average rate of 18kbit/s and a total length of 5Mbit.

6.4. Online QKD

After the successful offline QKD test, we proceeded with the final measurements demonstrating the real decoy-state QKD protocol. In total, we executed the online QKD protocol during three passes of the Chinese satellite. The first pass started on April 17th at 01:38h UTC (max. elevation 33°), the second on April 18th at 01:16h UTC (max. elevation 73°) and the third pass on April 19th at 00:54h UTC (max. elevation 48°). To evaluate the QBER, the sifted key rates and secure key rates, classical communication between the mission centre in China and the satellite is necessary for executing the post-processing steps for key-sifting, error correction and privacy amplification. Due to the limited bandwidth of the classical communication channel and the huge amount of data collected during the measurement campaign, many satellite passes over the mission centre are necessary. At the time of writing this report, the post-processing procedure has not been completed and thus we cannot report on the final results. However, we expect the results to be qualitatively and quantitatively similar to the results obtained during the offline QKD tests and they will be presented in the scientific publication of this work during the dissemination activities of the project.